



# Computational fluid dynamics (CFD) study of heat radiation from large liquefied petroleum gas (LPG) pool fires

Hang Yi<sup>a</sup>, Yu Feng<sup>a</sup>, Qingsheng Wang<sup>a,b,\*</sup>

<sup>a</sup> School of Chemical Engineering, Oklahoma State University, Stillwater, OK 74078, USA

<sup>b</sup> Mary Kay O'Connor Process Safety Center, Artie McFerrin Department of Chemical Engineering, Texas A&M University, College Station, TX 77843, USA



## ARTICLE INFO

### Keywords:

Liquefied petroleum gas (LPG)  
Pool fire  
Computational fluid dynamics (CFD)  
Radiation  
Safe separation distance

## ABSTRACT

Liquefied petroleum gas (LPG) is flammable and has risks of pool fires during its transportation, storage, and applications. The heat radiation by LPG pool fires poses hazards to individuals nearby and can lead to potential failures of ambient facilities. Due to the high costs and invasive nature of experiments for investigating large-scale pool fires, computational fluid dynamics (CFD) is employed in this study as the cost-effective and non-invasive method to simulate the process and analyze the characteristics of large hydrocarbon pool fires. Specifically, an experimentally validated 3-D CFD model has been built to simulate surface emissive power (SEP) and incident radiation of large-scale LPG pool fires with three different diameters and wind speeds. Steady-state simulations with P1 radiation and probability density function (PDF) combustion models were employed to obtain reliable data after the optimizations based on the comparisons with experimental data and empirical models. The comparison with benchmark experimental data demonstrates that the CFD model employed in this study can accurately predict the incident radiation of large LPG pool fires. A new SEP correlation is also proposed, which is specifically for LPG pool fires with a diameter between 10 m and 20 m. Additionally, the safe separation distances between LPG facilities and surrounded objects have been estimated based on the CFD simulation results. The high-resolution CFD model for large LPG pool fires in this work provides noninvasive and direct quantitative evidence to enhance the fundamental understanding on the safety of large LPG pool fires and can assist regulatory agencies in refining the safety limits in the cost-effective and time-saving manners.

## 1. Introduction

Liquefied petroleum gas (LPG) has been used widely in many applications, including utility, cooking, and heating appliances (Kojima, 2011). Potential risks need to be well controlled when using LPG. The risks include pool fires generated by the unintentional ignition on leaked LPG. The heat flux from the pool fire would increase personnel risks and cause significant damages to individuals, process equipment, storage tanks, and appliances (Pourdarvish et al., 2010; Mudan, 1984b). To reduce such risks, standards have been made and executed regulating the minimum separation distances from LPG facilities to exposures, and upper limits of thermal radiation to individuals or structures (McGrattan et al., 2000). However, there are discrepancies that need to be addressed and fine-tuned. For example, in the spacing requirements for LPG facility to its surroundings, the minimum space for LPG vaporizers to a container in NFPA 58 is 3 m (NFPA 58, 2014) and while in NFPA 59 is 15 m (NFPA 59, 2015). The thermal exposure criteria are also varying from different standards and regulations (NFPA

59A, 2016; API 521, 2014; 49 CFR, 2018; EN 1473, 2016) shown in Table 1.

Therefore, a better understanding of the radiated heat flux from LPG pool fires can provide not only essential information to manage the risks throughout the processes of production, transportation, and utilization, but also the high-resolution quantitative evidence to regulatory agencies to revise current requirements precisely. In the past decades, many experiments have been carried out to investigate the characteristics of hydrocarbon pool fires (Babrauskas, 1983 & 2002; Muñoz et al., 2004; Fu, 1973; May and McQueen, 2007; Cowley and Johnson, 1992), while none of them paid much attention to large LPG pool fires due to expensive costs and security considerations for experiment testing. Currently, CFD simulation method has become increasingly popular to be applied to investigate the properties of different fire scenarios (Joshi et al., 2016; Wang et al., 2016, 2018). Sinai and Owens (1995) employed CFD methods to analyze the impacts of pool shape, bund and ambient turbulence on the fire plume shape in kerosene pool fires. Rawat et al. (2002) used the unsteady flamelet

\* Corresponding author. Artie McFerrin Department of Chemical Engineering, Texas A&M University, College Station, TX 77843, USA.  
E-mail address: [qwang@tamu.edu](mailto:qwang@tamu.edu) (Q. Wang).

**Nomenclature**

$a$	Absorption coefficient
$A$	Surface area of the flame, $m^2$
$C$	Linear-anisotropic phase function coefficient
$D$	Pool diameter, m
$D_i$	Mass diffusivity of species $i$
$E$	Surface emissive power (SEP), $kW/m^2$
$E_{max}$	Equivalent ideal radiator emissive power of fuel, $kW/m^2$
$E_s$	Maximum smoke emissive power, $kW/m^2$
$E_{theory}$	Theoretical SEP, $kW/m^2$
$f$	Mass fraction
$F$	Geometric view factor
$f_{fuel}$	Mass fraction of the fuel stream
$f_{OX}$	Mass fraction of the oxygen
$f_{sec}$	Mass fraction of the secondary stream
$g_i$	Acceleration of gravity
$G$	Incident radiation in Eq. (12)
$G_b$	Generation of turbulence kinetic energy due to buoyancy
$G_k$	Generation of turbulence kinetic energy due to the mean velocity gradients
$h$	Mixture enthalpy
$H$	Flame height, m
$H'$	Flame height in inclined flame, m
$k$	Effective emission/absorption coefficient, /m
$k_1$	Average flame extinction coefficient
$k'_1$	Flame extinction coefficient
$k_G$	Reaction rate constant
$L$	Mean equivalent beam length of the flame, m
$\dot{m}$	Fuel mass burning rate, kg/s
$\dot{m}''$	Fuel burning rate per unit area, $kg/m^2 \cdot s$
$p$	Static pressure
$q_j$	Heat diffusion flux defined by Fourier's law
$\dot{q}''$	Total heat flux, $kW/m^2$
$\dot{q}'_{cond}$	Conductive heat transfer source, $kW/m^2$
$\dot{q}'_{conv}$	Convective heat transfer source, $kW/m^2$
$\dot{q}'_{rad}$	Radiative heat transfer source, $kW/m^2$
$Q$	Total energy radiated per unit time, kW
$r$	Radial distance from the source to the observer, m
$r'$	Radial distance from the fire flame center to the observer, m
$R$	Fire radius, m
$R_{IS}$	Radius of Iso-surface, m
$R_\epsilon$	User-defined source terms in Eq. (11)
$S_Q$	Energy source term
$S_\epsilon$	User-defined source terms in Eq. (11)
$t$	Time
$T_a$	Ambient temperature, K
$T_f$	Temperature of the radiator surface of the flame, K

$u_i$	Velocity component in the direction of Cartesian coordinate $x_i$
$u_w$	Wind velocity, m/s
$V_R$	Average percentage of velocity difference
$v_{m,n}$	Velocity at the reference point $m$ in mesh $n$ and mesh $m$
$v_{m,n+1}$	Velocity at the reference point $m$ in mesh $n+1$
$X_{LPG}$	Molar concentration of LPG
$X_{Oxidizer}$	Molar concentration of oxidizer
$Y_i$	Mass fraction of species $i$
$Y_M$	Contribution of the fluctuating dilatation in compressible turbulence to the overall dissipation rate
$Z_i$	Mass fraction for the $i$ -th element
$Z_{i,fuel}$	Mass fractions of LPG
$Z_{i,OX}$	Mass fractions of oxygen

**Greek Symbols**

$\beta$	Angle between the normal to the external objects
$\theta$	Flame inclined angle, °
$\rho$	Density
$\mu$	Dynamic viscosity
$\epsilon$	Emissivity ( $0 < \epsilon \leq 1$ )
$\sigma$	Stefan-Boltzmann constant which is equal to $5.6703 \times 10^{-8} J/m^2 \cdot s \cdot T^4$
$\tau$	Atmospheric transmissivity
$\tau_{ij}$	Constitutive relation for a Newtonian fluid
$\delta_{ij}$	Kronecker delta function
$\dot{\omega}_i$	Rate of formation of each species
$\dot{\omega}_{LPG}$	Rate of LPG consumed
$\alpha_\epsilon$	Inverse effective Prandtl numbers for $\epsilon$
$\alpha_k$	Inverse effective Prandtl numbers for $k$
$\chi_r$	Radiative fraction
$\Delta H_c$	Heat of combustion, kJ/kg

**Subscripts**

$m$	Number of the reference point
$n$	Mesh number
LPG	Liquefied petroleum gas
OX	Oxygen
sec	Secondary
f	Flame
a	Ambient
max	Maximum
s	Smoke
cond	Conduction
conv	Convection
rad	Radiation

approach to investigate the chemical reaction mechanisms of soot formation on a methane pool fire with 1 m diameter. Hostikka et al. (2003) used large-eddy simulation to simulate heat flux from methane pool fires ( $0.1 \text{ m} \leq D \leq 1 \text{ m}$ ) and found good agreements with experimental measurements. Small-size pool fires ( $D \leq 0.2 \text{ m}$ ) for gasoline, kerosene and tert-Butyl peroxybenzoate (TBPB) have been carried out to analyze the flame temperature and radiation of the corresponded pool fires (Attar et al., 2013). Sun et al. (2014 & 2015) used the large eddy simulation (LES) to analyze the radiated heat flux from LNG pool fires to estimate the distance between LNG tanks and vaporizers. Vasanth et al. (2015) found the exceptional agreement between experimental findings of pool fires situated at differing elevations and CFD simulations. Rengel et al. (2018) carried out a priori validation and found out that wind speeds and pool diameters are crucial factors influencing the

accuracy of the predictions from both codes of Flame Acceleration Simulator Fire and Fire Dynamics Simulation. This paper would have carried out the novel research of estimating the surface emissive power (SEP), predicting the incident radiation from large LPG pool fires to the surrounded objects, and proposing the reasonable minimum distances between the pool fire and objects using CFD simulations.

In this study, the characteristics of SEP and incident radiated heat flux of large LPG pool fires have been studied by using both empirical models and CFD simulations. Specifically, a 3-D CFD model has been built to estimate SEP and radiation from large LPG pool fires. The mesh independence test has been done first to ensure the optimized balance between computational accuracy and efficiency. Simulation results were compared with data from empirical models, and the CFD method has been validated by experimental measurements (Mudan, 1984a).

**Table 1**  
Thermal exposure criteria in standards and regulations.

Thermal radiation flux (kW/m <sup>2</sup> )	Conditions	Reference
5	Based on the quantitative assessment of both individual risk and social risk, it is equivalent to the consequence that no less than 10 individuals in open environment or at least one individual inside building, suffer second-degree skin burns on at least 10% of their bodies within 30 s of exposure to the thermal radiation.	NFPA 59A (2016)
32	Loss of strength of structural steel.	
9.46	Maximum heat flux at any location where urgent emergency action is required for individuals.	API 521 (2014)
6.31	Maximum heat flux in areas where emergency actions within 30 s are required for individuals without shielding but with proper clothing.	
4.73	Maximum heat flux in areas where emergency actions within 2–3 min are required by individuals without shielding but with proper clothing.	
1.58	Maximum heat flux at any location where individuals with proper clothing can be continuously exposed.	
5	A property line can be built to ignite a design spill.	49 CFR (2018)
9	The closest point of the structure outside the individual's property line	
30	A property line can be built upon for fire over an impounding area containing liquefied natural gas (LNG).	
32	The concrete outer surface of adjacent storage tanks.	EN 1473 (2016)
15	The outer mental surface of adjacent storage tanks.	
15	The outer surfaces of adjacent pressurized storage vessels and process facilities.	
8	Control rooms, maintenance workshops, laboratories, warehouses, etc.	
5	Administrative buildings.	
8	Remote area: An area only infrequently occupied by small numbers of persons.	
1.5	Critical area: This is either an unshielded area of critical importance where people without protective clothing can always be required, including during emergencies or urban area or a place difficult or dangerous to evacuate at limited time.	
5	Other areas: Other areas typically include industrial areas not under control of the operator/occupier of the liquefied natural gas LNG facilities.	

The specific separation distances between large LPG pool fires and ambient individuals/structures have been proposed based on the data from CFD simulations to satisfy the different codes and regulations. Additionally, a new correlated equation has been developed to predict the SEP for large LPG pool fires (10 m ≤ D ≤ 20 m).

## 2. Theory

### 2.1. Governing equations

#### 2.1.1. Conservation laws

In this study, conservations of mass, momentum, species balance, and energy, as well as key mechanisms of chemical kinetics (Faghri and Sundén, 2008) for turbulent reacting flows are discretized and solved in the simulation process. The above-mentioned governing equations are listed in Table 2.

#### 2.1.2. The Re-Normalization Group (RNG) k-ε model

The Re-Normalization Group (RNG) k-ε model is utilized to accurately predict the strained flows for LPG pool fire simulation in this study. The RNG k-ε model is also a computationally efficient, robust, and accurate model that can be applied for a wide range of turbulence flow simulations with heat transfer. Compared with similar Standard k-ε turbulence model, the RNG k-ε model considers the swirl flow and the improvement of the analytical formula for turbulent Prandtl numbers. The transport equations for the RNG k-ε model (Perry et al., 1984) are listed below:

$$\rho \frac{\partial k}{\partial t} + \rho \frac{\partial}{\partial x_i} (ku_i) = \frac{\partial}{\partial x_j} \left( \alpha_k \mu_{eff} \frac{\partial k}{\partial x_j} \right) + G_k + G_b - \rho \epsilon - Y_M + S_k \quad (10)$$

and

$$\rho \frac{\partial \epsilon}{\partial t} + \rho \frac{\partial}{\partial x_i} (\epsilon u_i) = \frac{\partial}{\partial x_j} \left( \alpha_\epsilon \mu_{eff} \frac{\partial \epsilon}{\partial x_j} \right) + C_{1\epsilon} \frac{\epsilon}{k} (G_k + C_{3\epsilon} G_b) - C_{2\epsilon} \rho \frac{\epsilon^2}{k} - R_\epsilon - S_\epsilon \quad (11)$$

### 2.2. Constitutive equations

#### 2.2.1. The P-1 radiation model

As the most simplified case of general P-N model, P-1 is based on the expansion of the radiation intensity into an orthogonal series of spherical harmonics (Cheng, 1964; Siegel and Howell, 1992). The radiation flux  $q_{rad}$  equation with four terms in the gray radiation model of LPG pool fire can be expressed as:

$$q_{rad} = -\frac{1}{3(a + \sigma_s) - C\sigma_s} \nabla G \quad (12)$$

#### 2.2.2. The non-premixed combustion model

LPG pool fire combustion should be considered as two separated streams (fuel vapor and air) from different sources in the modeling domain. ANSYS Fluent 19.2 (ANSYS, 2019) provides the non-premixed combustion model to simulate that fuel and oxidizer enter the reaction zone in distinct streams, and a fuel mass fraction  $f$  has been applied to this model. With this assumption, the mass fraction  $f$  (Sivathanu and Faeth, 1990) can be presented by

$$f = \frac{Z_i - Z_{i,OX}}{Z_{i,fuel} - Z_{i,OX}} \quad (13)$$

Since the composition of LPG in the United States is pure propane (Hahn, 2019), the mass fraction summation can be expressed as:

$$f_{fuel} + f_{sec} + f_{OX} = 1 \quad (14)$$

where  $f_{sec}$  is determined by  $f_{fuel}$  and  $f_{OX}$ .

#### 2.2.3. The surface emissive power (SEP) model

Surface emissive power (SEP),  $E$ , is defined as the heat flux due to heat radiation at the surface area of the flame. It can be computed with the Stefan-Boltzmann equation from an assumed gray radiator (Van den Bosch and Weterings, 2005) as follows:

$$E = \epsilon \sigma (T_f^4 - T_a^4) \quad (15)$$

The emissivity  $\epsilon$  for luminous and sooty flames, is often approximated by the equation (Drysdales, 2011)

$$\epsilon = 1 - \exp(-kL) \quad (16)$$

**Table 2**  
Conservations laws and chemical kinetics in the LPG pool fire modeling process.

Mass Conservation

$$\frac{\partial u_i}{\partial x_i} = 0 \tag{1}$$

Momentum

Conservation

$$\rho \frac{\partial u_i}{\partial t} + \rho \frac{\partial u_i u_j}{\partial x_j} = -\frac{\partial p}{\partial x_i} + \frac{\partial \tau_{ij}}{\partial j} + \rho g_i \tag{2}$$

$$\tau_{ij} = \mu \left( \frac{\partial u_i}{\partial x_j} + \frac{\partial u_j}{\partial x_i} \right) - \frac{2}{3} \mu \delta_{ij} \frac{\partial u_k}{\partial x_k} \tag{3}$$

Energy equation:

$$\rho \frac{\partial h}{\partial t} + \rho \frac{\partial}{\partial x_j} (u_j h) = \frac{\partial q_i}{\partial x_i} + \tau_{ij} \frac{\partial u_i}{\partial x_j} + \left( \frac{\partial p}{\partial t} + u_j \frac{\partial p}{\partial x_j} \right) + S_Q \tag{4}$$

Enthalpy of the gas mixture:

$$h = \sum_{i=1}^n h_i Y_i \tag{5}$$

Energy Conservation

Heat diffusion flux:

$$q_j = \lambda \frac{\partial T}{\partial x_j} + \rho \sum_{i=1}^n h_i \left( D_i \frac{\partial Y_i}{\partial x_j} \right) \tag{6}$$

Species Balance

$$\rho \frac{\partial Y_i}{\partial t} + \rho \frac{\partial}{\partial x_j} (u_j Y_i) = \rho \frac{\partial}{\partial x_j} \left( D_i \frac{\partial Y_i}{\partial x_j} \right) + \dot{\omega}_i \tag{7}$$

Chemical Kinetics



$$\dot{\omega}_{LPG} = \frac{d[X_{LPG}]}{dt} = -k_G(T)[X_{LPG}]^n [X_{Oxidizer}]^m \tag{9}$$

Note: The terms from left to right in momentum equation are unsteady term, convection term, pressure gradient, diffusion term, and gravity term, respectively; the terms from left to right in mixture enthalpy are unsteady term, convection term, diffusion term, dissipation term, compressibility term, and heat source term, respectively; in the mass fraction equation, the terms from left to right are unsteady term, convection term, diffusion term, and rate of information source term, respectively.

where  $L$  has a slight relationship with the flame geometry of LPG pool fires, is approximately equal to the fire radius  $R$ . In this paper, the fire flame is assumed as a back body, and  $\varepsilon = 1$ .

In some circumstances, the flame temperature and emission/absorption coefficient data are not available. Another method (Van den Bosch and Weterings, 2005) was come up that SEP is appropriate to theoretical SEP,  $E_{theory}$ , determined by the heat of combustion with the surface area of the flame expressed by

$$E_{theory} = \frac{\chi_r \dot{Q}}{A} \tag{17}$$

and

$$\dot{Q} = \dot{m} \Delta H_C \tag{18}$$

where  $\chi_r$  is related to C/H of fuel compounds (Koseki, 1989) and pool diameters (McCaffrey and Harkleroad, 1989); previous numerical studies (Souil et al., 1984; Fleury, 2010; Delichatsios, 1993; Yang et al., 1994; Quintiere and Grove, 1988; Cox, 1995) presented that the radiative fraction of propane fire flames ranges from 0.28 to 0.35; and the flame surface area  $A$  is determined the flame height  $H$  and fire diameter  $D$ , i.e.,

$$A = \frac{\pi D^2}{2} + \pi D H \tag{19}$$

In the single-zone solid model, the averaged SEP can be determined using the fraction of energy radiated from pool fires (Mudan, 1984b; Yang et al., 1994; Moorhouse and Pritchard, 1982) given by the following equation

$$E = \frac{\chi_r \dot{m}' \Delta H_C}{1 + 4H/D} \tag{20}$$

Using the initial fire design and evaluation method, Ufuah and Bailey (2011) proposed a correlation for SEP which can be expressed by

$$E = 70 \exp(-k_1 D) \tag{21}$$

where  $k_1 = 0.00165 \text{ m}^{-1}$ .

Mudan and Croce (1988) obtained a uniform model for SEP of flames for smoky hydrocarbons as follows:

$$E = E_{max} \exp(-k_1' D) + E_s (1 - \exp(1 - k_1' D)) \tag{22}$$

where  $E_{max} = 140 \text{ kW/m}^2$ ,  $E_s = 20 \text{ kW/m}^2$ , and  $k_1' = 0.2 \text{ m}^{-1}$ .

In this study, the empirical models would have been combined with results of CFD simulations to estimate the SEP in large LPG pool fires.

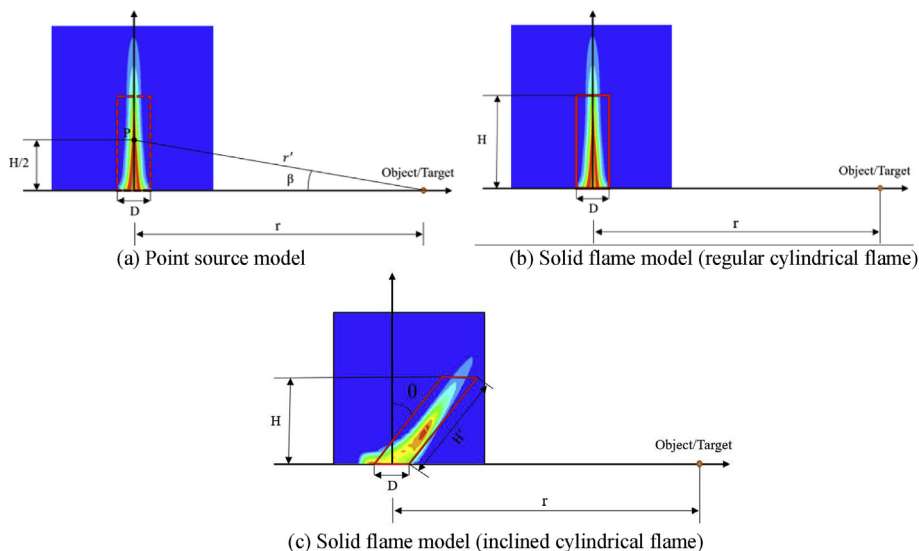


Fig. 1. Point source model (PSM) and solid flame model (SFM) to calculate incident radiation from LPG pool fires.

Specifically, after comparing with the experimental measurements, a new correlation was developed to predict the SEP in large LPG pool fires ( $10\text{ m} \leq D \leq 20\text{ m}$ ) properly.

### 2.2.4. Radiated heat flux generated by LPG pool fires

The radiated heat flux generated by LPG pool fires consists of the contributions of conduction, convection, and radiation (see Eq. (23)). The semi-quantitative equation to compute heat flux was obtained by [Hottel \(1958\)](#) as follows:

$$\dot{q}'' = \dot{q}''_{conv} + \dot{q}''_{cond} + \dot{q}''_{rad} \quad (23)$$

In Eq. (23), the radiative heat flux plays a significant role in the heat flux from pool fires to objects, while other terms such as conductive and convective heat transfer sources are ignored in existing studies ([Mudan, 1984b](#); [Drysdale, 2011](#); [Fay, 2006](#)).

To predict  $\dot{q}''_{rad}$  from pool fires, the widely accepted point source model (PSM) and the solid flame model (SFM) are often applied. Specifically, PSM is the most applicable configuration model to calculate the radiation heat flux at any distance from the pool fire source with the equation

$$\dot{q}''_{rad} = \frac{\chi_r \dot{Q}}{4\pi r^2} \quad (24)$$

[Drysdale \(2011\)](#) correlated PSM with the information of the narrow-angle radiometer data for the radiative heat flux to the external target (see [Fig. 1 \(a\)](#)) with the equation

$$\dot{q}''_{rad} = \frac{\chi_r \cos\beta \dot{Q}}{4\pi r'^2} \quad (25)$$

where  $\beta$  is the angle between the normal to the external objects and the line of sight between the object and point source, and  $r'$  is determined by  $r$  and  $H$ . Specifically,

$$r' = \sqrt{\frac{H^2}{4} + r^2} \quad (26)$$

SFM ([Mudan, 1984b,1987](#)) is another widely used model for describing radiative heat flux,  $\dot{q}''_{rad}$ , to outside targets (see [Fig. 1 \(b\) & \(c\)](#)) around the pool fire expressed by

$$\dot{q}''_{rad} = EF\tau \quad (27)$$

where  $F$  is geometric view factor, and  $\tau$  is atmospheric transmissivity.

## 3. Numerical method

### 3.1. Geometry

A 3-D computational domain for a large LPG pool fire at the center has been constructed, with a pool diameter of 16.9 m (see [Fig. 2](#)). The O-Grid blocking strategy was employed the finite volume mesh generation of the cylindrical flame region using ICEM CFD 19.2 ([ANSYS, 2019](#)), which is also shown in [Fig. 2](#). In order to obtain the final mesh for the simulation, the mesh independence test was conducted with four sets of meshes with different mesh densities. The total mesh cell numbers of the four meshes are 1,184,477 (Mesh 1), 2,885,631 (Mesh 2), 3,694,746 (Mesh 3) and 5,029,535 (Mesh 4).

A mesh independence test was performed by refining the mesh until the average percentage of velocity difference  $V_R$  was less than 1% between mesh iterations. Specifically,  $V_R$  is employed (see Eq. (28)) to compare the velocity magnitudes at different locations in Z-axis direction at the LPG mass flow rate of 44.37 kg/s ([Mudan, 1984a](#)). On plane  $Z = 0$ , 50 locations have been selected which are randomly distributed in the flow domain. The velocity magnitudes at the locations have been acquired and compared. Specifically,  $V_R$  can be calculated by:

$$V_R = \frac{\sqrt{\sum_{m=1}^{50} \left( \frac{v_{m,n+1} - v_{m,n}}{v_{m,n+1}} \right)^2}}{50} \quad (28)$$

where  $n$  is the mesh index ( $n = 1,2,3,4$ ). Based on the mesh independence test results shown in [Fig. 3](#), Mesh 3 provides the optimum balance between computational efficiency and accuracy. Specifically,  $V_R$  reaches the minimum due to the lowest summation of truncation and round-off errors. Therefore, Mesh 3 was employed as the final mesh for this study.

### 3.2. Numerical setup

Finite volume method is used to discretize the computational domain and solve the governing equations in the CFD simulations. RNG k- $\epsilon$  method ([Perry et al., 1984](#)) is used as turbulence model, and the P-1

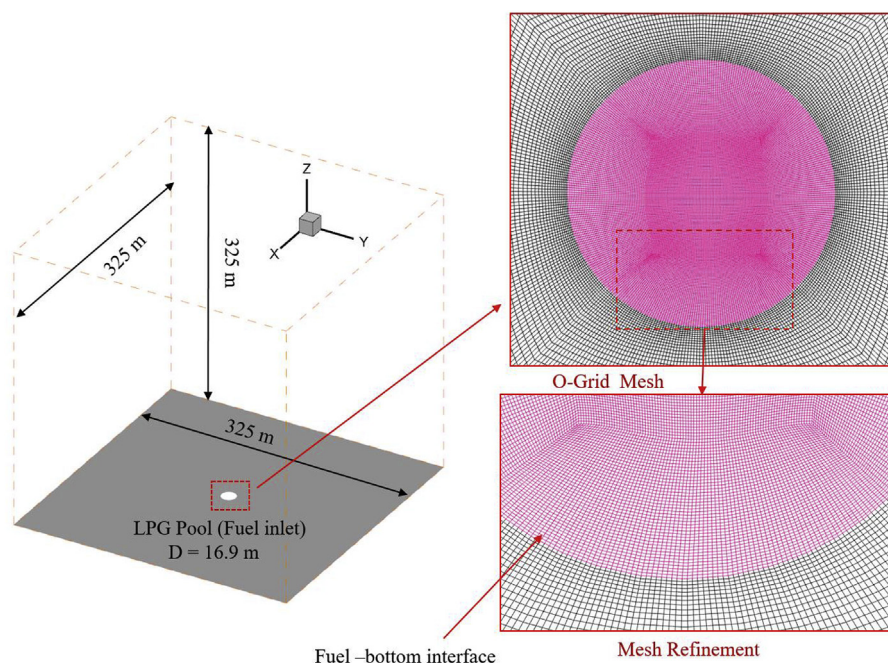


Fig. 2. LPG pool fire geometry and the structured hexahedral mesh ( $D = 16.9\text{ m}$ ).

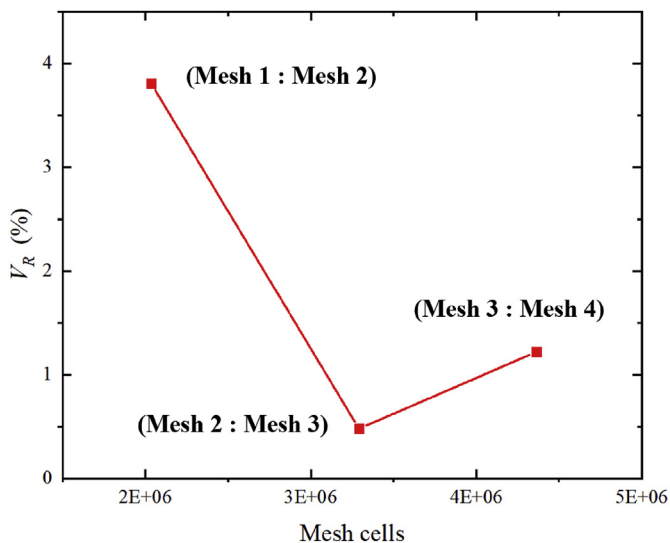


Fig. 3. Comparisons of  $V_R$  in different meshes for mesh independence test.

**Table 3**  
Boundary conditions of the CFD simulation for large LPG pool fires.

Pool diameter (m)	Atmosphere temperature (K)	Mass burning rate (kg/s)	Wind velocity (m/s)
12.9	309	29.087	3
14.9	306	47.328	2.5
16.9	312	44.426	0

model (Cheng, 1964; Siegel and Howell, 1992) is selected as the radiation model. Using the fuel stream rich flammability limit and boundary species in the species transport model, the non-premixed combustion method is employed to simulate LPG pool fire with the calculated probability density function (PDF) table. To investigate the pool size effect, the mesh has been scaled with factors of 0.882 and 0.763 for the pools with 12.9 m and 14.9 m in diameters, respectively. Boundary conditions were determined based on the experimental measurements (Mudan, 1984a) and are listed in Table 3.

The numerical solution of the governing equations with appropriate

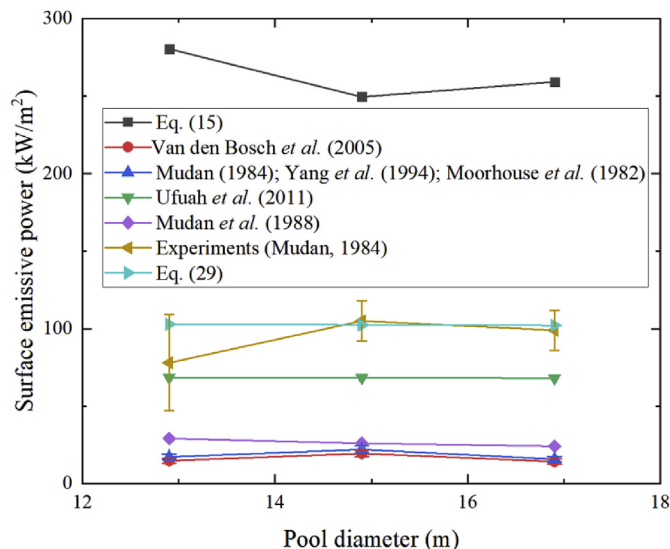


Fig. 5. Comparison of surface emissive power ( $\text{kW/m}^2$ ) obtained by empirical models, proposed equation, and experiments for large LPG pool fires.

boundary conditions was performed by using a user-enhanced, commercial finite-volume based program, i.e., ANSYS Fluent 19.2 (ANSYS, 2019). All variables, including velocity components, pressure, shear rates, and species concentrations, were calculated and located at the centroids of the discretized mesh cells. Simulations were run on a local 64-bit Dell Precision Tower 7810 with 128 GB of RAM and 3.40 GHz processors. Second-order upwind schemes were adopted to discretize the governing equations of mass, momentum, turbulent kinetic energy, turbulent dissipation rate, energy, mean mixture fraction, and mixture fraction variance. The coupled scheme was employed for pressure-velocity coupling, and the least squares cell-based scheme was applied to spatial discretization. To evaluate the convergence, the residuals assigned are  $1e-6$  for energy and P1, and  $1e-3$  for the other governing equations.

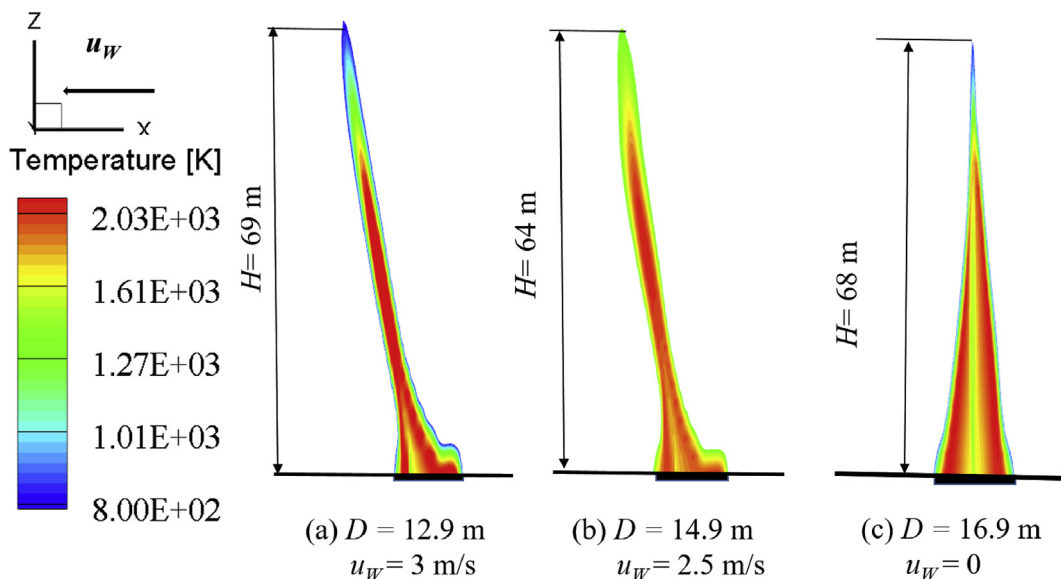


Fig. 4. Temperature (K) profiles of large LPG pool fires in different sizes and atmosphere conditions: (a)  $D = 12.9$  m,  $u_w = 3$  m/s, (b)  $D = 14.9$  m,  $u_w = 2.5$  m/s, (c)  $D = 16.9$  m,  $u_w = 0$ .

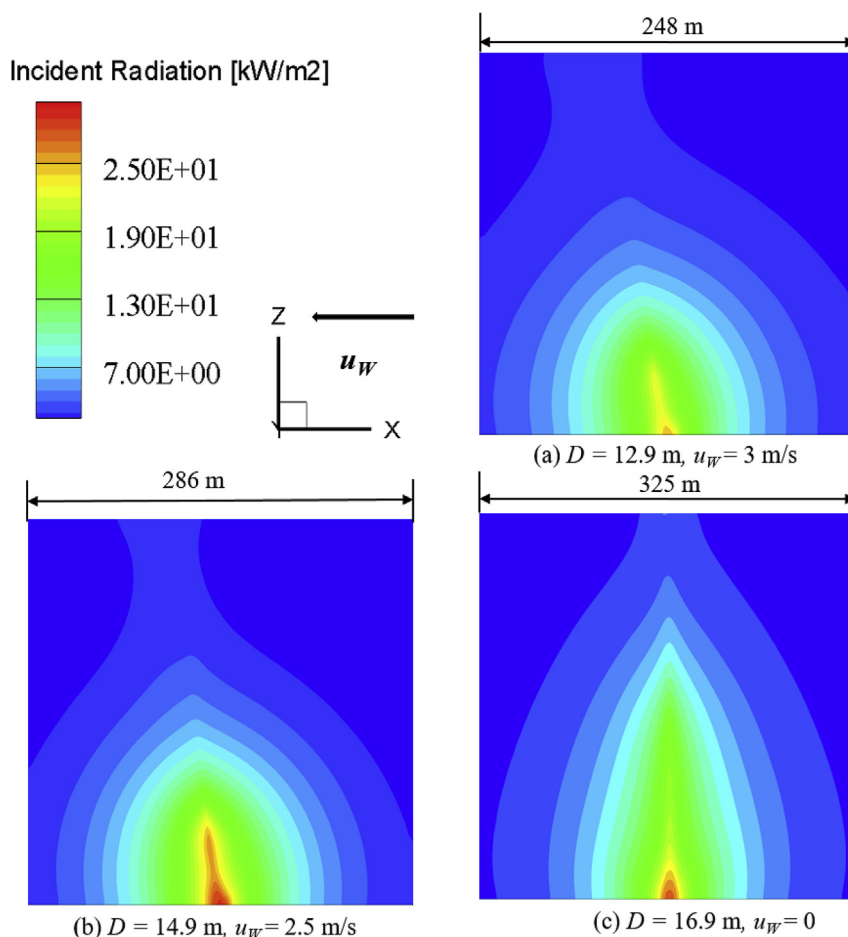


Fig. 6. Incident radiation distributions at  $Y = 0$  of large LPG pool fires with different sizes and wind speeds: (a)  $D = 12.9$  m,  $u_w = 3$  m/s, (b)  $D = 14.9$  m,  $u_w = 2.5$  m/s, (c)  $D = 16.9$  m,  $u_w = 0$ .

## 4. Results and discussion

### 4.1. Surface emissive power (SEP)

To find the flame temperature  $T_f$  and flame height  $H$  which are used to calculate the SEP and radiated heat flux from large LPG pool fires by empirical models, the temperature profiles of the three LPG pool fires from CFD simulations are obtained which are shown in Fig. 4 (a) to (c). Hägglund and Persson (1976) claimed that the distinguished temperature for fire flames from the black smoke body is 800 K. In this paper, the LPG pool fire scenario is considered as steady-state. Accordingly, steady-state CFD solver was employed for the numerical study. Therefore, the temperature is applied in this paper to differ the flame zone to smoke zone. The average flame temperatures 1492, 1449 and 1492 K in the large LPG pool fires with the corresponded diameters 12.9, 14.9 and 16.9 m have been used to calculate the SEP in Eq. (15). The flame heights in the three large LPG pool fires have been employed to Eq. (17), Eq. (20), Eq. (25), as well as Eq. (27). Therefore, with the data obtained from CFD simulations, the empirical models can be validated to estimate the SEP and radiative heat flux from large LPG pool fires.

Using the flame heights and temperatures obtained from Fig. 4, the SEP for the large LPG pool fires have been obtained by the empirical models, and have been compared with experimental data (Mudan, 1984a) shown in Fig. 5. Fig. 5 demonstrates that Eq. (21) provide the best SEP prediction compared with the experimental data. While other equations generate noticeable deviations when estimating the SEP for large LPG pool fires. Equation (15) overestimates the SEP, which is more than two times over the experimental results, and for other

equations, such as Eqs. (17), (20) and (22), the results from these equations, are appropriate while they underestimate SEP from large LPG pool fires. The main factor for the large errors is the inaccurate extrapolation from small-scale experiments to large-scale fires when generating the empirical models. Another possible factor is because existing models were not developed specifically for LPG pool fires. Nevertheless, the results obtained by Eq. (21) show that it has a similar trend with the experiment results to predict the SEP for large LPG pool fires. Therefore, to further reduce the relative errors between Eq. (21) and experiment measurements, a new equation has been proposed in this study based on the research of Ufuah and Bailey (2011) as follows:

$$E = 105 \exp(-k_1 D) \quad (10 \text{ m} \leq D \leq 20 \text{ m}) \quad (29)$$

where  $k_1 = 0.00165 \text{ m}^{-1}$ .

Comparisons of SEPs between numerical studies using Eq. (29) and benchmark experimental data are shown in Fig. 5. The comparison shows that Eq. (29) provides more accurate predictions than other empirical models with less relative errors of the estimated SEP in large LPG pool fires with the pool diameters employed in this study (see Table 3). It is worth mentioning that the composition of LPG in the United States is pure propane (Hahn, 2019), while the compositions are different in other countries. Therefore, Eq. (29) is limited to be used in large LPG pool fires with 100% propane. A more generalized SEP correlation for large LPG pool fires will be developed in the future.

### 4.2. Radiative heat flux

Fig. 6 (a) to (c) show the distribution of incident radiation that is

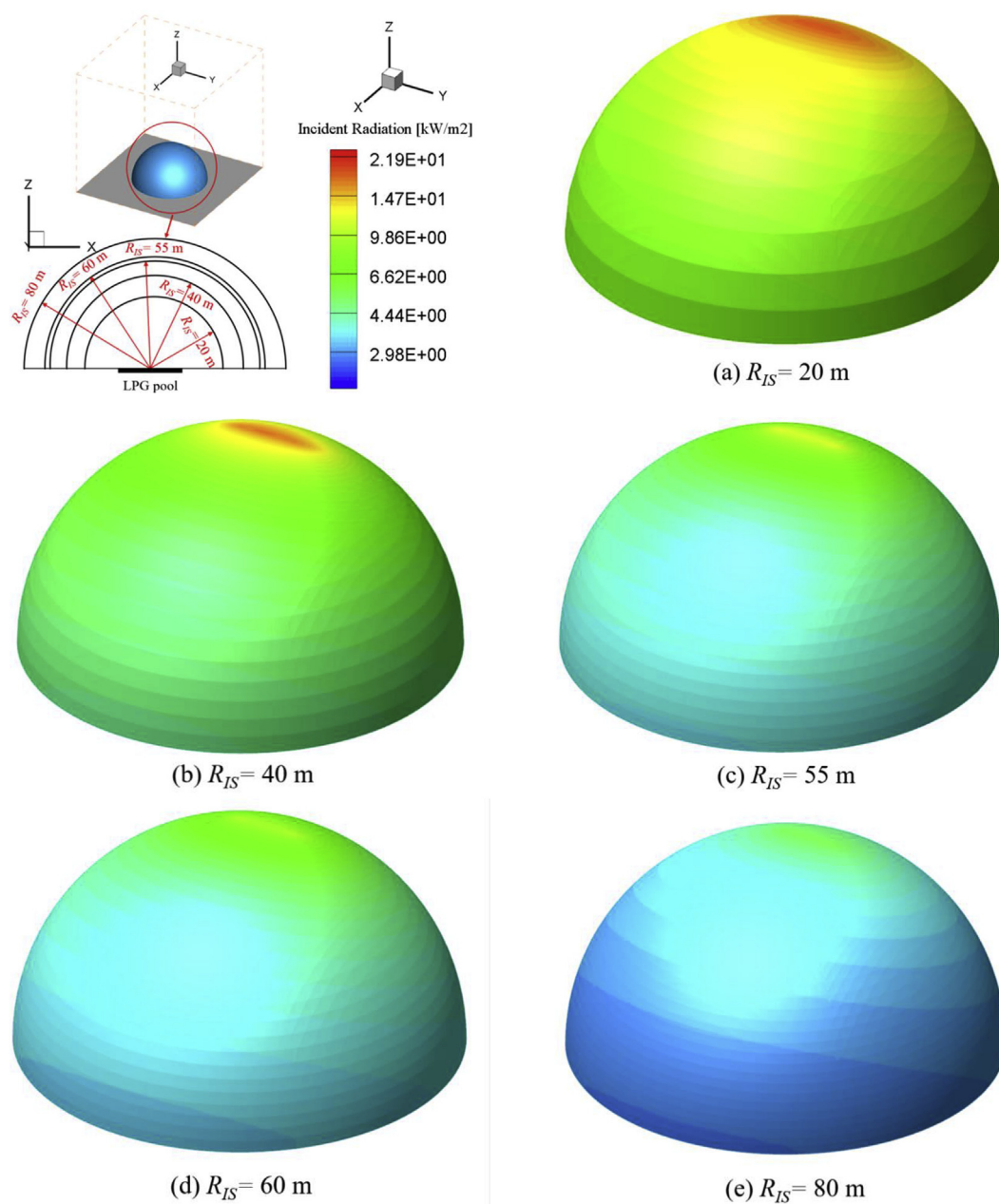


**Fig. 7.** Iso-surfaces of incident radiation ( $\text{kW/m}^2$ ) at different  $R_{IS}$  in LPG pool fire ( $D = 12.9$  m): (a)  $R_{IS} = 20$  m, (b)  $R_{IS} = 40$  m, (c)  $R_{IS} = 55$  m, (d)  $R_{IS} = 60$  m, (e)  $R_{IS} = 80$  m.

obtained by CFD simulations in large LPG pool fires with the different diameters and wind speeds. The maximum incident radiation for these pool fires is  $22.90 \text{ kW/m}^2$ ,  $27.58 \text{ kW/m}^2$ , and  $30.87 \text{ kW/m}^2$ , respectively. It can be observed from Fig. 6 that the maximum incident radiation for the pool fire ( $D = 12.9$  m) is smaller than another two pool fires. It might be due to the factor of the burning rate, which is only  $29.087 \text{ kg/s}$  and much less than the corresponding values of LPG pool fires with the diameters of  $14.9$  m and  $16.9$  m. Fig. 6 also demonstrates that the wind has a significant impact on incident radiation distribution. The incident radiation is tilted towards the wind direction, and the tilting angle increases with wind speed. The reason for the incident radiation leaning to air direction is because of the enhanced convection of evaporated components released from the LPG pool. Thus, the incident radiation distribution is determined by the shape of fire flame (see Fig. 4), which is formed by the distribution of evaporated LPG after its burning.

To obtain the incident radiation at different distances ( $R_{IS}$ ) to the center of the LPG pool fire, Iso-surfaces colored by the radiation magnitude have been visualized in Figs. 8–10. Specifically, the Iso-surfaces are generated  $R_{IS} = 20, 40, 50, 60,$  and  $80$  m for all three different large LPG pool fires.  $R_{IS}$  values were selected to facilitate the comparisons between the CFD simulation results and the experimental data (see Fig. 10). Although no experimental data for incident radiation are currently available at  $R_{IS} = 20$  m, simulation results at that distance were still acquired to study distribution conditions of the incident radiation close to the pool fire burning area. Figs. 6 and 7(a), 8(a), 9(a), and 10 integrally demonstrate that the average incident radiation at  $R_{IS} = 20$  m are higher than  $10 \text{ kW/m}^2$  in all three pool fires, which can potentially lead to severe damages to the individuals in this area (API 521, 2014). Further post-processing of the high-resolution incident radiation distributions can provide quantitative evidence and guide fire departments on how to protect our firefighters from heat radiation risks

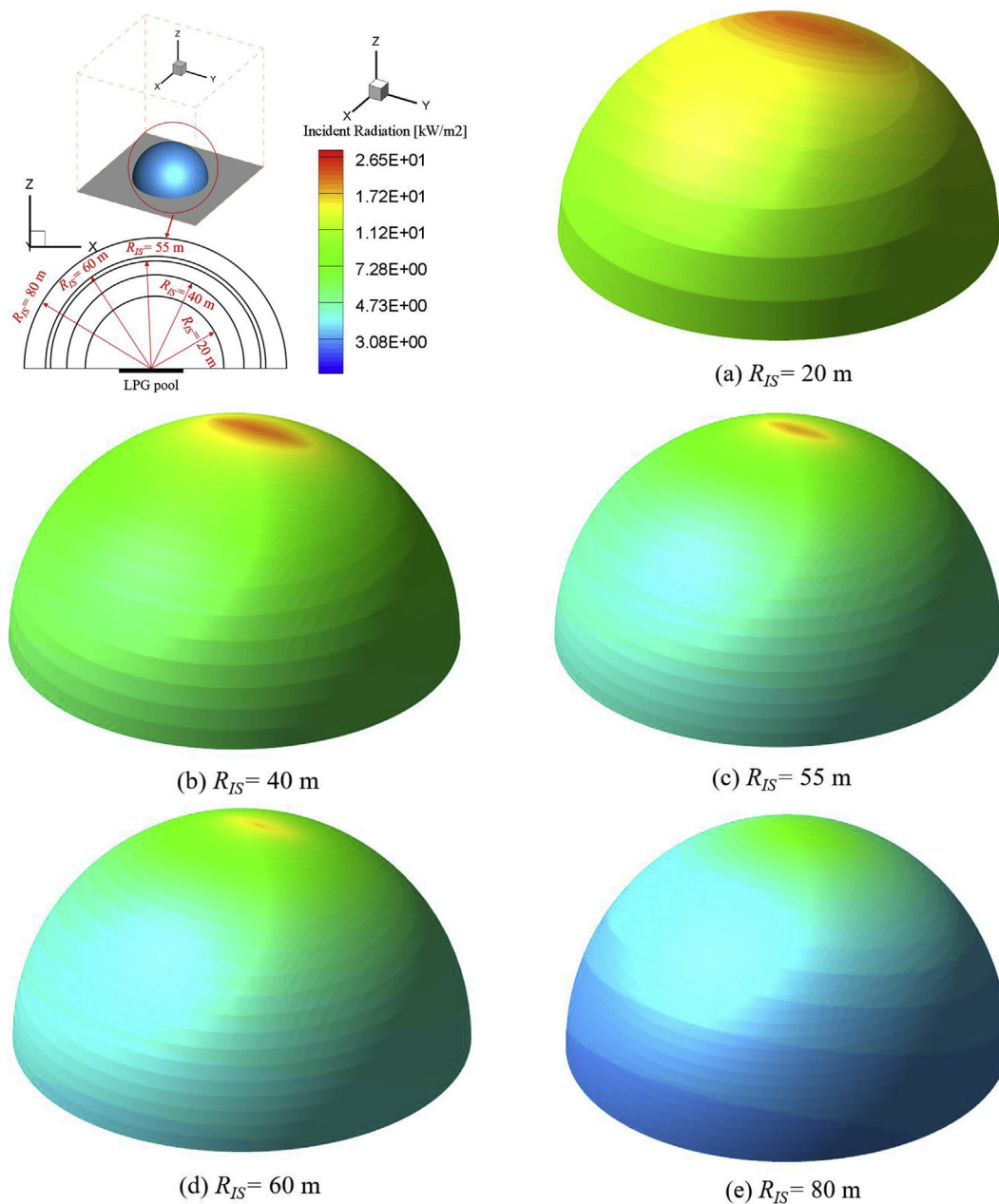


Fig. 8. Iso-surfaces of incident radiation ( $\text{kW/m}^2$ ) at different  $R_{IS}$  for LPG pool fire ( $D = 14.9\text{ m}$ ): (a)  $R_{IS} = 20\text{ m}$ , (b)  $R_{IS} = 40\text{ m}$ , (c)  $R_{IS} = 55\text{ m}$ , (d)  $R_{IS} = 60\text{ m}$ , (e)  $R_{IS} = 80\text{ m}$ .

when approaching centers of large LPG pool fires.

It should also be noticed that the highest incident radiation magnitudes locate near the tops of Iso-surfaces, with deviations due to different tilting effects driven by the wind. To understand specific radiation behaviors more systematically, the maximum and average incident radiations of each Iso-surface have been obtained, and these results are compared with experimental results and data from empirical models (see Fig. 10 (a) to (c)). From Figs. 7–10, it can be found that the CFD model employed in this study provides the best accuracy on predicting the incident radiation of large LPG pool fires, compared with existing empirical models. In Fig. 10, it shows that SFM (see Eq. (27)) has better performance to estimate incident radiation from large LPG pool fires than PSM (see Eq. (15)), and the results from SFM present a similar trend with the maximum values of CFD simulation. Despite that the experimental data for the pool fire ( $D = 14.9\text{ m}$ ) may have noticeable fluctuations when measuring incident radiations, the CFD simulation results show the great fitting with the experiments on radiation

distribution from a distance between 20 m and 80 m in the pool fire ( $D = 14.9\text{ m}$ ). Exceptions on good agreements between numerical and experimental data exist at  $R_{IS} = 40\text{ m}$  which also can be observed in another two LPG pool fires. In Fig. 10, it can be observed that the airflow condition has a significant impact on the heat radiation distribution from 45 m to 60 m to the pool fires with diameters 12.9 m and 14.9 m. High wind velocity might also influence the measurement accuracy of the thermocouples in the experiments, which is a possible reason for the deviations between CFD and experimental data with high ambient airflow velocities. Without the wind velocity effects, good agreements between experimental data and CFD results can be seen in Fig. 10 in the static air condition with the pool diameter 16.9 m. Based on the good overall predictions of the CFD simulation results, the CFD model and the numerical results can be used to estimate the safe separation distances between large LPG pool fires and targets properly.

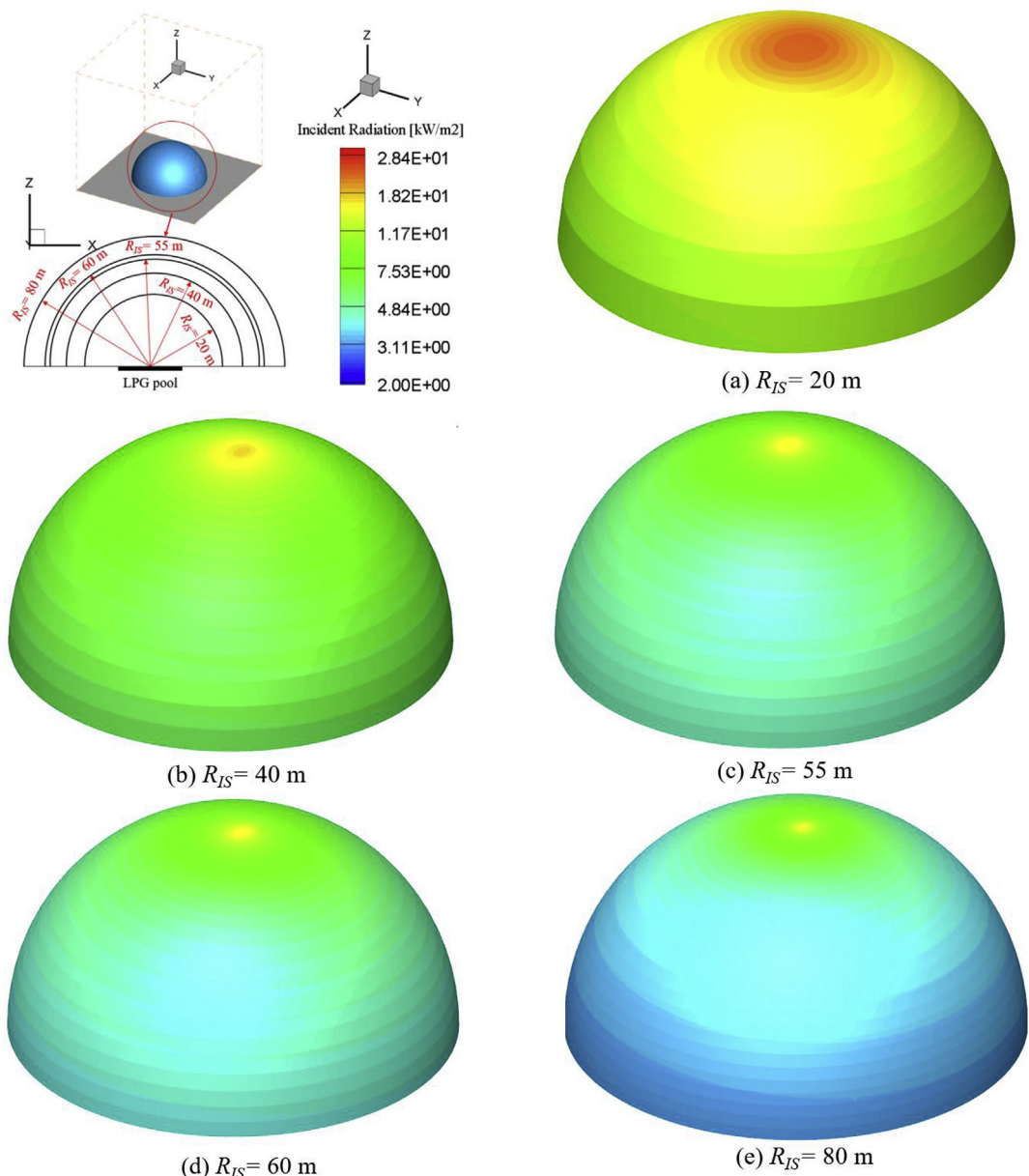


Fig. 9. Iso-surfaces of incident radiation (kW/m<sup>2</sup>) at different  $R_{IS}$  for LPG pool fire ( $D = 16.9\text{ m}$ ): (a)  $R_{IS} = 20\text{ m}$ , (b)  $R_{IS} = 40\text{ m}$ , (c)  $R_{IS} = 55\text{ m}$ , (d)  $R_{IS} = 60\text{ m}$ , (e)  $R_{IS} = 80\text{ m}$ .

### 4.3. Safe separation distance

In Table 1, it shows that the maximum safe thermal exposure is 1.5 kW/m<sup>2</sup> to individuals in the unshielded area or urban area. While from Figs. 6–10, it can be found that the minimum radiated heat flux is larger than 2 kW/m<sup>2</sup> in the simulated three LPG pool fires. Thus, the radiation from a longer distance ( $R_{IS} > 80\text{ m}$ ) must be considered for appropriate safety distance estimation. Fig. 11 shows the maximum and average incident radiations from 20 m to 160 m for these three LPG pool fires. It can be observed that the maximum incident radiation for all pool fires is strongly influenced by the shape of fire flames (see Figs. 4 and 5) because the wind speed can dominantly impact the flame morphologies. Average incident radiations share similar distributions from 20 m to 160 m around the pool fires. In contrast, the incident radiation distribution trends are different from the pool fire morphology when the ambient airflow field is static. The maximum incident radiation decreases slowly from 50 m to 100 m away from the center of the pool fire with the diameter 16.9 m, while the maximum

radiated heat flux drops rapidly from 50 m to 100 m for the pool fires with the diameters 12.9 m and 14.9 m which might be due to wind condition. Airflow condition would have a significant impact on the fuel evaporation morphologies which determine the shape of fire flame. Moreover, the air velocity has a negligible effect on the distribution trend of the average incident radiation because the total energy generated by the pool fire is similar and determined by the fuel-burning rate.

Using the data and simulation results shown in Table 1 and Fig. 11, the safe separation distances of LPG pool fires to the surrounded targets can be estimated. Large LPG pool fires tend to more likely happen in an outdoor environment rather than indoor area because only limited LPG is allowed to be utilized and stored in buildings and structures (NFPA 58, 2014), and the limited LPG is not available to form a large LPG pool. Indeed, the horizontal radiated heat flux draws more safety concerns than the vertical component due to the fact that individuals and facilities are often located on the ground around the pool fire accidents. Therefore, the average incident radiation was chosen as the more

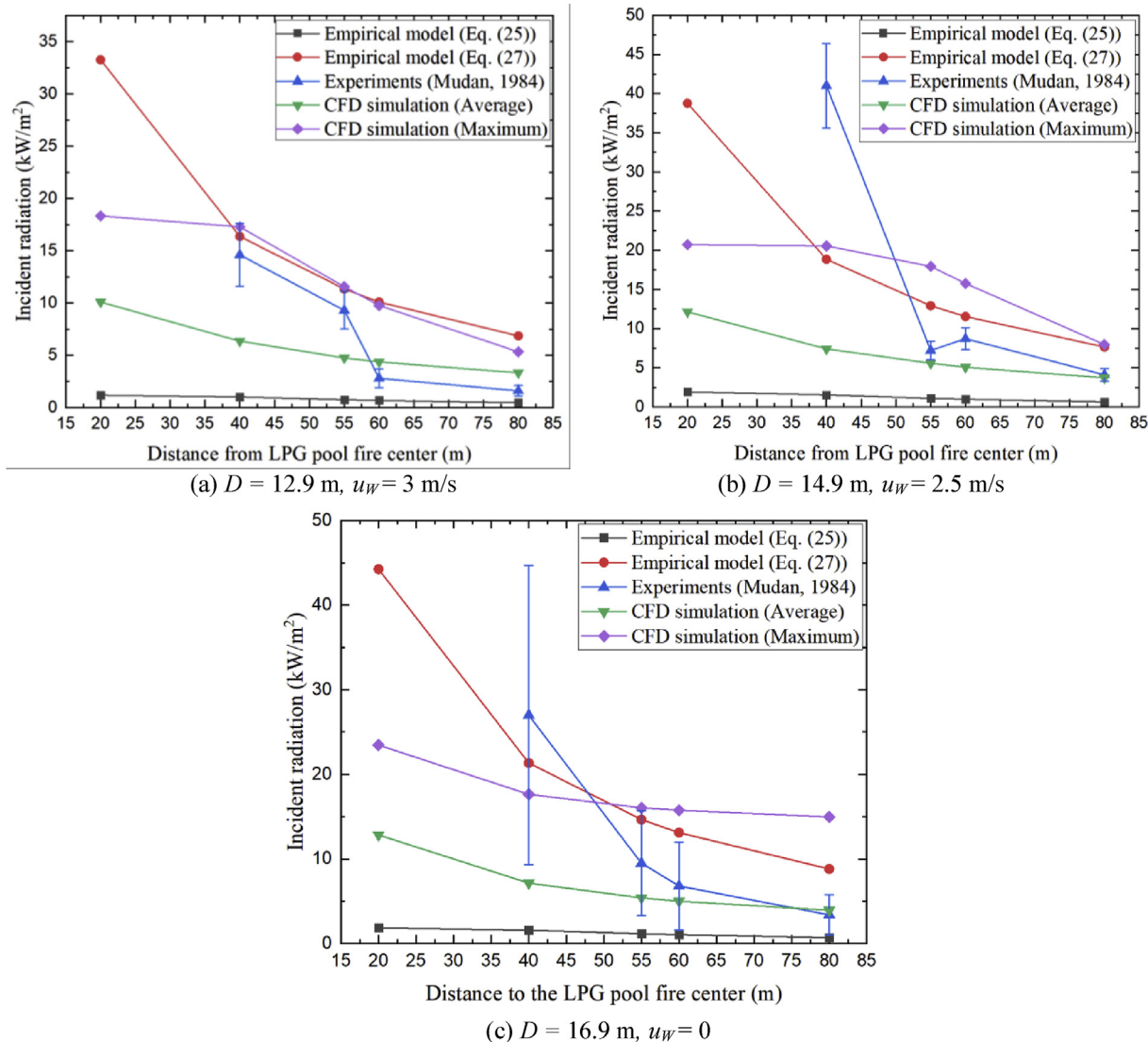


Fig. 10. Comparison of incident radiation (kW/m<sup>2</sup>) among empirical models, experimental data and CFD simulations in large LPG pool fires under different diameters: (a)  $D = 12.9$  m,  $u_w = 3$  m/s, (b)  $D = 14.9$  m,  $u_w = 2.5$  m/s, (c)  $D = 16.9$  m,  $u_w = 0$ .

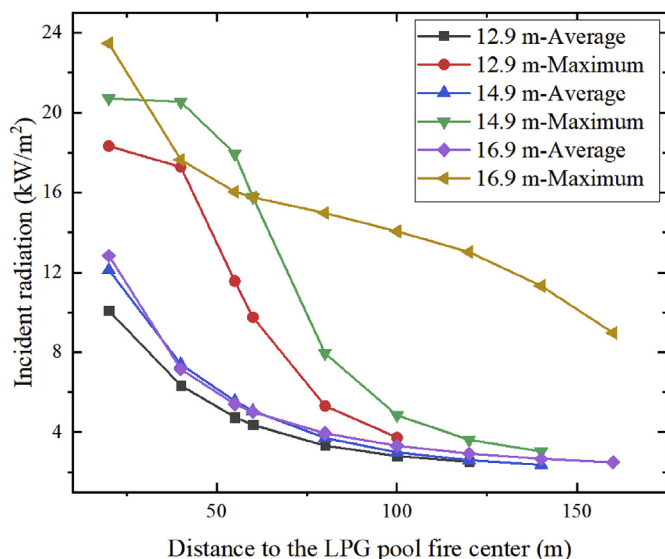


Fig. 11. The maximum/average incident radiation predicted by CFD simulations for large LPG pool fires.

appropriate parameter to estimate safe separation distances than the maximum incident radiation, which is weighted more by the vertical radiation component.

Using the CFD simulation tool developed in this study, the estimated safe separation distance between LPG pool fires and targets for each code with corresponded pool fires are listed in Table 4. For the regulations and standards (NFPA 59A, 2016; 49 CFR, 2018; 1473, 2016), the upper limit of the thermal exposure is larger than 15 kW/m<sup>2</sup> for these objects, such as structures, concrete surface to adjacent storage tanks, mental surface to adjacent storage tanks, outer surfaces of adjacent pressurized storage vessels etc. Thus, it is difficult to obtain the safe separation distances in these objects because the maximum predicted average radiation is only 12.85 kW/m<sup>2</sup>. However, the safe separation distance can be less than 20.0 m, based on the fact that the maximum predicted average radiation is 12.85 kW/m<sup>2</sup> in the simulation results of this study. In contrast, the thermal exposure limit is 1.5 kW/m<sup>2</sup> for the individuals wearing appropriate protections under continuous exposure conditions (49 CFR, 2018) and the critical area (EN 1473, 2016), such as an unshielded area of critical importance where people without protective clothing. Since the exposure limit (49 CFR, 2018) is lower than the minimum average incident radiations predicted by the CFD simulation (2 kW/m<sup>2</sup>). Therefore, the safe

**Table 4**  
Safe separation distances between large LPG pool fires and targets estimated using CFD simulations.

Code	Targets	Advised safe separation distance (m)		
		$D = 12.9\text{ m}$	$D = 14.9\text{ m}$	$D = 16.9\text{ m}$
NFPA 59A (2016)	Individuals	52.0	60.0	61.0
	Structures	< 20.0	< 20.0	< 20.0
API 521 (2014)	Individuals (Urgent emergency)	23.0	31.5	31.0
	Individuals (Action in 30s)	40.5	45.0	48.0
	Individuals (Action in 2 min–3 min)	54.0	63.5	63.5
49 CFR (2018)	Individuals (No action needed)	> 120.0	> 140.0	> 160.0
	To ignite a design spill	52.0	60.0	60.0
	Individual's property	25.5	33.0	33.0
	An impounding area containing LNG	> 120.0	> 140.0	> 160.0
EN 1473 (2016)	Concrete surface to adjacent storage tanks	< 20.0	< 20.0	< 20.0
	Metal surface to adjacent storage tanks and outer surfaces of adjacent pressurized storage vessels	< 20.0	< 20.0	< 20.0
	Control rooms et al. and remote area	30.5	36.0	37.0
	Administrative buildings and other areas	52.0	60.0	61.0
	Critical area	> 120.0	> 140.0	> 160.0

Note: The detailed descriptions for the targets are presented in Table 1.

separation distance determined by 49 CFR (2018) and EN1473 (2016) should be farther than 120 m, 140 m and 160 m for the LPG pool fires with the diameters of 12.9 m, 14.9 m and 16.9 m, respectively. Generally, the specific safe separation distances for other codes can also be obtained using the CFD simulation data by following the similar analysis procedures mentioned above. Thus, the results from CFD simulation could provide valuable data for the code committees to evaluate the risks from large LPG pool fires.

## 5. Conclusions

In this study, a new correlation is provided and integrated with the CFD simulations to predict the SEP, the incident radiation, and safe separation distances of large LPG pool fires. Simulation results were compared with existing experiments. In CFD simulation, the RNG  $k-\epsilon$  model was applied to turbulence simulation as it has been validated to be more effective than the Standard  $k-\epsilon$  model. Moreover, with the advantages of P-1 radiation model and non-premixed combustion model, it is more reliable and accurate to describe the scenarios of large LPG pool fires. Based on the empirical models and experimental data, a new correlation for SEP in LPG (100% propane) pool fire ( $10\text{ m} \leq D \leq 20\text{ m}$ ) has been proposed in this paper, which provides better prediction accuracies than existing models. CFD simulations show that the airflow conditions have less impact on maximum and average incident radiations to the surrounding individuals and structures, which are determined by the burning rate of LPG pool fires. However, the airflow condition would have significant impacts on the distribution of incident radiation in the same iso-surfaces, and it would tilt to wind direction because radiative heat flux distribution is determined by the flame configuration. Based on available results from CFD simulations, the safe separation distances have been suggested under the requirements of different codes. Therefore, it can be concluded that the incident radiation from CFD simulations can help us to have better understandings and estimations of the safe separation distances. The CFD model developed in this study can predict the radiative heat flux from large LPG pool fires and assess the relevant exposure health risks.

## Acknowledgments

The research was partially sponsored by the Fire Protection Research Foundation, United States. The use of ANSYS software (Canonsburg, PA) as part of the ANSYS-CBBL academic partnership agreement is gratefully acknowledged (Dr. Thierry Marchal, Global Industry Director). Some of the computing for this project was performed at the OSU High-Performance Computing Center at Oklahoma

State University (Dr. Dana Brunson, Director and Dr. Evan Linde, Research Cyberinfrastructure Analyst).

## References

- 49 CFR, 2018. Liquefied Natural Gas Facilities, vol. 193.
- ANSYS, 2019. ANSYS Inc. (Canonsburg, PA).
- API Standard 521, 2014. Pressure-relieving and Depressuring Systems, sixth ed. .
- Attar, A.A., Pourmanhdian, M., Anvaripour, P., 2013. Experimental study and CFD simulation of pool fires. *Int. J. Comput. Appl.* 70 (11), 9–15.
- Babrauskas, V., 1983. Estimating large pool fire burning rate. *Fire Technol.* 19 (4), 251–261.
- Babrauskas, V., 2002. third ed. Heat Release Rate. *SPFE Handbook of Fire Protection Engineering*, vol. 3. National Fire Protection Association, Quincy, MA, Section, pp. 1–37.
- Cheng, P., 1964. Two-dimensional radiating gas flow by a moment method. *Am. Inst. Aeronaut. Astronaut. J.* 2, 1662–1664.
- Cowley, L.T., Johnson, A.D., 1992. Oil and Gas Fires: Characteristics and Impact, Offshore Technology Information. OTI Report No. 596, UK Health and Safety Executive. (Berkshire).
- Cox, G., 1995. Combustion Fundamentals of Fire. Academic Press, London.
- Delichatsios, M., 1993. Transition from momentum to buoyancy controlled turbulent jet diffusion flames and flame height relationships. *Combust. Flame* 92 (4), 349–364.
- Drysdale, D., 2011. An Introduction to Fire Dynamics, third ed. John Wiley & Sons, NY.
- EN 1473, 2016. Installation and Equipment for Liquefied Natural Gas-Design of On-Shore Installations.
- Faghri, M., Sundén, B., 2008. Transport phenomena in fires. In: *WIT Transactions on State-Of-The-Art in Science and Engineering*.
- Fay, J.A., 2006. Model of large pool fire. *J. Hazard. Mater.* B136, 219–232.
- Fleury, R., 2010. Evaluation of Thermal Radiation Models for Fire Spread between Objects. Master Thesis, University of Canterbury, Australia.
- Fu, T.T., 1973. Heat radiation from fires of aviation fuels. *Fire Technol.* 10 (1), 54–67.
- Hägglund, B., Persson, L.E., 1976. The Heat Radiation from Petroleum Fires. *Forsvarets Forskningsanstalt, Stockholm*.
- Hahn, E., 2019. LPG gas mixture of propane & butane: which gas is present in LPG. [online]. Available: <https://www.elgas.com.au/blog/1972-lpg-contains-which-gases-gases-present-in-lpg-gases-used>, Accessed date: 5 July 2019.
- Hostikka, A., McGrattan, K.B., Hamins, A.P., 2003. Numerical modeling of pool fires using LES and finite volume method for radiation. In: *Fire Safety Science-Proceedings of the Seventh International Symposium*, pp. 383–394.
- Hottel, H.C., 1958. Review of certain laws governing the diffusive burning of liquids. *Fire Res. Abstracts Rev.* 1, 41–44.
- Joshi, P., Bikini, P., Wang, Q., 2016. Consequence analysis of accidental release of supercritical carbon dioxide from high pressure pipelines. *Int. J. Greenh. Gas Control* 55, 166–176.
- Kojima, M., 2011. The Role of Liquefied Petroleum Gas in Reducing Energy Poverty: Extractive Industries and Development Series #25. World Bank, Washington, DC [online]. Available: <http://documents.worldbank.org/curated/en/39066146815779954/The-role-of-liquefied-petroleum-gas-in-reducing-energy-poverty>, Accessed date: 12 January 2011.
- Koseki, H., 1989. Combustion properties of large liquid pool fires. *Fire Technol.* 25 (3), 241–255.
- May, W.G., McQueen, W., 2007. Radiation from large liquefied natural gas fires. *Combust. Sci. Technol.* 7 (2), 51–56.
- McCaffrey, B.J., Harkleroad, M., 1989. Combustion efficiency, radiation, CO and soot yield from a variety of gaseous, liquid, and solid fueled buoyant diffusion flames. In: *Symposium on Combustion*, vol. 22. pp. 1251–1261 (1).
- McGrattan, K.B., Baum, H.R., Hamins, A., 2000. Thermal Radiation from Large Pool Fires

- (NISTIR 6546). National Institute of Standards and Technology, MD.
- Moorhouse, J., Pritchard, M.J., 1982. Thermal Radiation Hazards from Large Pool Fires and Fireballs. European Federation of Chemical Engineering Publication Series, pp. 397–428.
- Mudan, K.S., 1984a. Hydrocarbon Pool and Vapor Fire Data Analysis. USDOE Report No. DE-AC01-83EP16008. US Department of Energy, Washington DC.
- Mudan, K.S., 1984b. Thermal radiation hazards from hydrocarbon pool fires. *Prog. Energy Combust. Sci.* 10 (1), 59–80.
- Mudan, K.S., 1987. Geometric view factors for thermal radiation hazard assessment. *Fire Saf. J.* 12 (2), 89–96.
- Mudan, K., Croce, P., 1988. Fire hazard calculations for large open hydrocarbon fires. In: first ed. SFPE Handbook of Fire Protection Engineering, vol. 2. National Fire Protection Association, Quincy, MA, Section, pp. 45–87.
- Muñoz, M., Arnaldos, J., Casal, J., Plana, E., 2004. Analysis of geometric and radiative characteristics of hydrocarbon pool fires. *Combust. Flame* 139, 263–277.
- NFPA 58, 2014. Liquefied Petroleum Gas Code.
- NFPA 59, 2015. Utility LP-Gas Plant Code.
- NFPA 59A, 2016. Standard for the Production, Storage, and Handling of Liquefied Natural Gas (LNG).
- Perry, R.H., Gree, D.W., Maloney, J.O., 1984. Perry's Chemical Engineers' Handbook, sixth ed. McGraw-Hill, NY.
- Pourdarvish, R., Khajehnajafi, S., Cowles, C., 2010. The Many Faces of Fire Hazards in Industrial Settings. *Occupational Health & Safety* [online]. Available: <https://ohsonline.com/articles/2010/12/01/the-many-faces-of-fire-hazards-in-industrial-settings.aspx>, Accessed date: 12 January 2010.
- Quintiere, B.S., Grove, J.G., 1988. A unified analysis for fire plumes. In: *Symptom (International) Combustion*, vol. 27. pp. 2757–2766 (2).
- Rawat, R., Pitsch, H., Ripoll, J.F., 2002. Large-eddy simulation of pool fires with detailed chemistry using an unsteady flamelet model. In: *Proceedings of the Summer Program*, pp. 357–367.
- Rengel, B., Mata, C., Pastor, E., Casal, J., Planas, E., 2018. A priori validation of CFD modelling of hydrocarbon pool fires. *J. Loss Prev. Process. Ind.* 56, 18–31.
- Siegel, R., Howell, J.R., 1992. Thermal Radiation Heat Transfer. Hemisphere Publishing Corporation, Washington DC.
- Sinai, Y.L., Owens, M.P., 1995. Validation of CFD modelling of unconfined pool fires with cross-wind: flame geometry. *Fire Saf. J.* 24 (1), 1–34.
- Sivathanu, Y.R., Faeth, G.M., 1990. Generalized state relationships for scalar properties in non-premixed hydrocarbon/air flames. *Combust. Flame* 82, 211–230.
- Souil, J., Joulain, P., Gengembre, E., 1984. Experimental and theoretical study of thermal radiation from turbulent diffusion flames to vertical target surfaces. *Combust. Sci. Technol.* 41 (1–2), 69–81.
- Sun, B., Guo, K., Pareek, V.K., 2014. Computational fluid dynamics simulation of LNG pool fire radiation for hazard analysis. *J. Loss Prev. Process. Ind.* 29, 92–102.
- Sun, B., Guo, K., Pareek, V.K., 2015. Dynamic simulation of hazard analysis of radiations from LNG pool fire. *J. Loss Prev. Process. Ind.* 35, 200–210.
- Ufua, E., Bailey, C.G., 2011. Flame radiation characteristics of open hydrocarbon pool fires. In: *Proceeding of the World Congress on Engineering*, vol. III (London).
- Van den Bosch, C.J.H., Weterings, R.A.P.M., 2005. Methods for the Calculation of Physical Effects: Due to Releases of Hazardous Materials (Liquids and Gases), 'yellow Book'. Sdu Uitgevers, The Hague CPR 14E [in two parts].
- Vasanth, S., Tauseef, S.M., Abbasi, T., Abbasi, S.A., 2015. CFD simulation of pool fires situated at differing elevation. *Process Saf. Environ. Protect.* 94, 89–95.
- Wang, Z., Wang, W., Wang, Q., 2016. Optimization of water mist droplet size by using CFD modeling for fire suppressions. *J. Loss Prev. Process. Ind.* 44, 626–632.
- Wang, W., He, T., Huang, W., Shen, R., Wang, Q., 2018. Optimization of switch modes of fully enclosed platform screen doors during emergency platform fires in underground metro station. *Tunn. Undergr. Space Technol.* 81, 277–288.
- Yang, J.C., Hamins, A., Kashiwagi, T., 1994. Estimate of the effect of scale on radiative heat loss fraction and combustion efficiency. *Combust. Sci. Technol.* 96, 183–188.